An effective modelling and control strategy for linear switched reluctance motors

S W Zhao[1], **N C Cheung**[1*], **W C Gan**[2], and **J M Yang**[3]

[1]Department of Electrical Engineering, Hong Kong Polytechnic University, Kowloon, Hong Kong, People's Republic of China

[2]Motion Group, ASM Assembly Automation Hong Kong Ltd, Kwai Chung, NT, Hong Kong, People's Republic of China

[3]Electric Power College, South China University of Technology, Guangzhou, People's Republic of China

The manuscript was received on 11 October 2007 and was accepted after revision for publication on 19 May 2008.

DOI: 10.1243/09544062JMES904

Abstract: Trajectory control is an essential element in advanced manufacturing processes. For demanding direct-drive applications, a linear switched reluctance motor (LSRM) has become a potential candidate because of its low cost and simple structure. However, the inherent non-linearities of the LSRM cause difficulties in its controller design. Recently, a few complicated control approaches and schemes have been proposed to overcome the non-linear characteristics, but they need precise modelling, and their algorithms are hard to realize. This article describes a simple and effective design of the feedback control for the trajectory control of the LSRM driving system, and some of its practical aspects. In the proposed control algorithm, the whole driving system is decomposed into two subsystems with different time scales by using the two-time-scale analysis. On the basis of this method, the position controller and current controllers are designed for the two subsystems, respectively. In this way, the controller structure is simplified and the whole tracking system can be designed tractable. Furthermore, a modified proportional-differential controller is proposed for tracking the sinusoid wave. This article includes modelling analysis, simulation results, and detailed experimental implementation as well.

Keywords: linear switched reluctance motor, trajectory control, two-time-scale analysis

1 INTRODUCTION

The linear switched reluctance motors (LSRMs) have drawn much research attention over the past decade, due to its low cost, simple structure, ruggedness, reliability in harsh environments and its potential for numerous industrial applications. Compared with the method of rotary motors having mechanical transformation components for producing linear motion, LSRM has many advantages, such as quick response, high sensitivity, and precise tracking capability. Moreover, the structure of an LSRM can reduce the space requirement for its installation. In addition, LSRM has a simpler construction, more rugged structure and lower system cost than that of a direct-drive permanent magnet linear synchronous motor. These advantages make LSRM an alternative choice for direct-drive applications. However, the main limitations for the LSRM come from its inherent non-linear characteristics and force-ripple output. The non-linear characteristics are due to its non-linear force function of position and current and the effect of magnetic saturation. These problems create difficulties in the controller design of the LSRM drive system.

Rotary switched reluctance motors (RSRMs) have a longer history than LSRM and therefore most control methods in literature are originally designed for the RSRM. General foundations for the practical design of a family of switched reluctance motors (SRMs) are investigated in reference [**1**]; it demonstrates that machines in this family can provide the basis for fully-controllable variable speed systems. In reference [**2**], a flux linkage-based controller is proposed for an RSRM and experimental results show that low torque

Corresponding author: Department of Electrical Engineering, Hong Kong Polytechnic University, Hunghom, Kowloon, Hong Kong, People's Republic of China. email: eencheun@inet.polyu.edu.hk; norbert.cheung@polyu.edu.hk

ripple can be achieved over a range of speed and torques. In reference [**3**], a reduced-order model is proposed for controller design and the non-linear torque compensation is implemented using a lookup table. Two feedback linearization controllers are designed for position and speed tracking in references [**4**] and [**5**], where a full order non-linear model is applied. In references [**6**] and [**7**], two adaptive controllers are proposed to combat the non-linear characteristics of the motor by using the online estimation. In the area of LSRM control, the speed control LSRM are discussed in references [**8**] to [**10**]. Precision position-related control is reported in references [**11**] and [**12**]. In reference [**11**], the authors adopt a lookup table to linearize the relationships among phase force, current and position and a plug-in compensator to improve the system robustness. A closed-form solution is further developed for short-distance position control in reference [**12**]. These control schemes can achieve high performance; but the complicated non-linear control algorithms require a high-performance processor and dedicated sensors for full implementation. In addition, building a lookup table, especially a high-precision lookup table, from vast experimental data would require considerable time.

The objective of here is to propose a relatively simple controller design, which can be conveniently realized on a low-cost embedded system for trajectory control applications. Hence, this article adopts an approximated reduced-order model and a simple and effective controller strategy for LSRM. These measures are tailor-made for implementation in embedded systems at a very low cost. The whole driving system is decomposed into an electrical sub-system and a mechanical sub-system with different time scales. The position controller and current controller are designed individually for the two sub-systems in a cascaded structure. In order to obtain smooth force output, a winding excitation scheme consisting of a force distribution function (FDF) and an approximated function of inductance ratio, usually is used to connect the two sub-systems. Besides, a modified proportional–differential (PD) controller on the basis of the previous work [**11**], which is insensitive to frequency variations in low-frequency bandwidth, is proposed to improve the sinusoid wave tracking ability of the system.

2 MODELLING AND CONTROLLER DESIGN OF LSRM

2.1 Configuration and modelling of LSRM

In this article, the proposed LSRM is a three-phase motor. The design schematic of the LSRM system

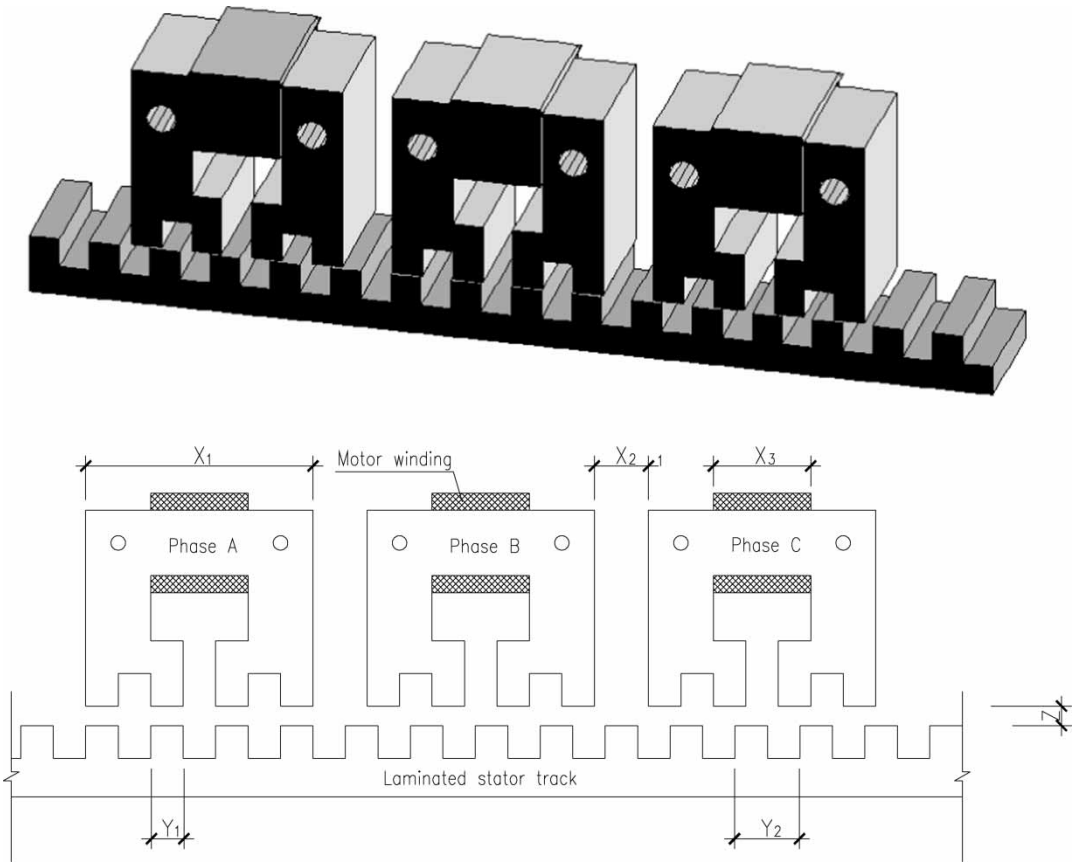

Fig. 1 Schematic of the LSRM

Table 1 The electrical and mechanical parameters of the LSRM

Pole width (y_1)	6 mm
Pole pitch (y_2)	12 mm
Motor length (x_1)	146 mm
Phase separation (x_2)	10 mm
Wind width	25 mm
Air gap width (z)	0.5 mm
Phase resistance	1.5 Ω
Aligned inductance	10.2 mH
Unaligned inductance	7.8 mH
Mass of the moving platform (M)	1.8 kg
Friction constant (B)	0.08 N s m/s

is shown in Fig. 1. Its electrical and mechanical parameters are listed in Table 1. A set of three-phase coils with the same dimensions is installed on the moving platform. The body of the moving platform is manufactured with aluminium so that the total weight of the moving platform is low and the magnetic paths are decoupled. The moving platform is mounted on two slider blocks that are tightly fixed to the bottom of the LSRM. This rugged mechanical structure can effectively buffer extend vibration during its operation.

The dynamic behaviour of the whole system can be determined by Kirchhoff's law of the voltage balance of individual phase coil and by Newton's law of the motor's mechanical motion. The equations of LSRM can be expressed as voltage equation (1) and mechanical equation (2). Since the flux linkage is a function of current and position, the voltage equation can be further expressed as in equation (3), in which the second term on the right-hand side corresponds to the voltage drop due to the position movement, and the third term corresponds to the one due to the current change. Thus

$$V_j = r_j i_j + \frac{\mathrm{d}\lambda_j}{dt}, \qquad j = a, b, c \tag{1}$$

$$f_\mathrm{e} = M\frac{\mathrm{d}^2 x}{\mathrm{d}t^2} + B\frac{\mathrm{d}x}{\mathrm{d}t} \tag{2}$$

and

$$V_j = r_j i_j + \frac{\partial \lambda_j}{\partial x}\frac{\mathrm{d}x}{\mathrm{d}t} + \frac{\partial \lambda_j}{\partial i_j}\frac{\mathrm{d}i_j}{\mathrm{d}t}, \qquad j = a, b, c \tag{3}$$

where V_j is the applied voltage to phase j, i_j is the corresponding current, r_j is the resistance and λ_j is its flux linkage; f_e is the electromechanical force produced and x is the displacement of the moving platform. The mass of the moving platform M and the system friction constant B can be measured directly.

The connection between the two equations is the force producing function by which the energy of the system is transferred from an electromagnetic to a mechanical form. The total electromechanical force is the sum of the individual electromechanical forces as given in equation (4). The force f_j produced by phase j is determined by differentiating the co-energy function with respect to the position as in equation (5) [**13**]. The force produced is a non-linear function of the position and phase current. Further, it can be seen that the force is a non-linear function, even though the magnetic circuit operates in its linear region, in which the phase-force produced can be rewritten as equation (6). Here, L_j is named phase inductance being the ratio of the phase flux linkage by its current. The highly non-linear characteristics of the driving system are therefore due to its non-linear flux behaviour and the mechanism of force origination

$$f_\mathrm{e} = \sum_{j=a}^{c} f_j \tag{4}$$

$$f_j = \frac{\partial}{\partial x}\int_0^{i_j} \lambda_j \,\mathrm{d}i_j \tag{5}$$

$$f_j = \frac{1}{2}\frac{\mathrm{d}L_j}{\mathrm{d}x} i_j^2 \tag{6}$$

The response times of the electromagnetic behaviour and mechanical motion are quite different. Based on this fact the singular perturbation theory-based two-time-scale analysis [**3**] is applied to the model and to design the driving system. Assuming that terminal voltage for each phase is regulated by equation (7), the voltage equation (3) can be rewritten in the standard singular perturbation form as equation (8).

$$V_j = K_i(i_{jd} - i_j), \qquad j = a, b, c \tag{7}$$

$$\varepsilon\frac{\mathrm{d}i_j}{\mathrm{d}t} = \left(\frac{\partial \lambda_j}{\partial i_j}\right)^{-1}\left[i_{jd} - i_j - \varepsilon\left(r_j i_j - \frac{\partial \lambda_j}{\partial x}\frac{\mathrm{d}x}{\mathrm{d}t}\right)\right], \quad j = a, b, c \tag{8}$$

where K_i denotes the proportional coefficient for of the current control, i_{jd} denotes the desired current and $\varepsilon = K_i^{-1}$. The whole driving system can be seperated into two sub-systems with different time-scales, named fast and slow sub-systems. In the t-scale, the slow sub-system can be expressed as equation (2) corresponding to the mechanical motion. In this situation, the steady currents are taken into consideration by setting $\varepsilon = 0$ in equation (8). The fast sub-system describes the dynamical electromagnetic behaviours of the coil by introducing a stretched time variable as given in (9). In the τ-scale, the fast sub-system is represented as equation (10) by treating the variables of slow subsystem as constants.

$$\tau = \frac{t}{\varepsilon} \tag{9}$$

$$\frac{\mathrm{d}i_j}{\mathrm{d}\tau} = \left(\frac{\partial \lambda_j}{\partial i_j}\right)^{-1}(i_{jd} - i_j), \qquad j = a, b, c \tag{10}$$

To satisfy this two-time-scale analysis, an adequately large K_i should be applied to ensure the reasonable separation of time scale. This is justified for our test set-up, since the current loop bandwidth can be achieved up to kHz while the output mechanical bandwidth is in the order of 10 Hz [**11**]. In this framework, the fast sub-system is considered by the treatment of the variables of slow sub-systems as invariable. It is also reasonable to describe the slow sub-systems as the variables of the fast sub-system in their steady states. For a trajectory control system the slow subsystem is a second-order differential equation (2) from the input of total force to the output of the position. The fast sub-system is a first-order differential equation (3) for current control.

Through this analysis the complicated driving system can be divided into two tractable reduced-order sub-systems and it is possible to design controllers of each sub-system, respectively. This is the essential first step in designing the simple yet effective control algorithms for LSRM.

2.2 Commutation strategy

Commutation is one of the essential tasks for the controller. The desired force performance of an LSRM is always carried out by the synchronous commutation with its current position. However, commutation is associated with the problem of force ripples. To obtain smooth output force a force sharing strategy [**8**, **11**], which is similar to the torque sharing approach for SRMs [**4**, **6**], can be applied to weaken the force ripples of single-phase excitation. For any given position, there are two sets corresponding to the phases positive-force produced and negative-force produced as follows

$$\Theta^+ = \left\{ j : \frac{\partial L_j(x)}{\partial x} \geqslant 0 \right\} \quad \text{and} \quad \Theta^- = \left\{ j : \frac{\partial L_j(x)}{\partial x} < 0 \right\}$$

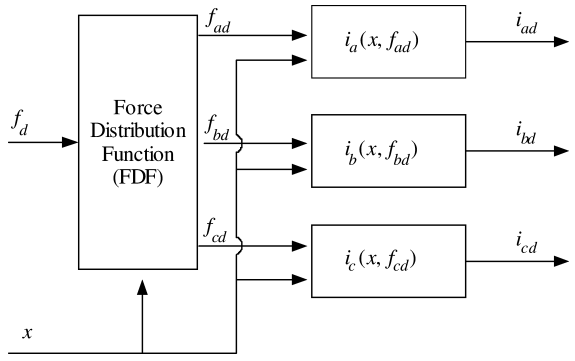

Fig. 2 The diagram of a motor winding excitation scheme

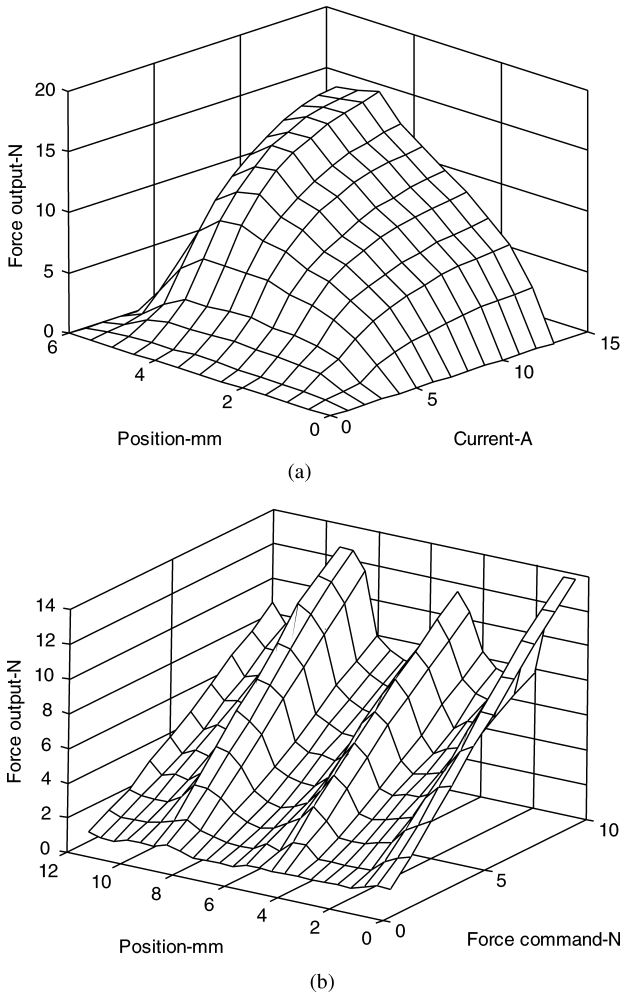

Fig. 3 (a) Experimental data of current versus position versus force output three-dimensional chart for single phase and (b) experimental force command versus position versus force output three-dimensional chart for force sharing strategy

Table 2 The FDF scheme

Position range	Positive force command	Negative force command
0–2 mm	$f_{bd} = f_d$	$f_{cd} = 0.5(2-x)f_d, f_{ad} = 0.5xf_d$
2–4 mm	$f_{bd} = 0.5(4-x)f_d, f_{cd} = 0.5(x-2)f_d$	$f_{ad} = f_d$
4–6 mm	$f_{cd} = f_d$	$f_{ad} = 0.5(6-x)f_d, f_{bd} = 0.5(x-4)f_d$
6–8 mm	$f_{cd} = 0.5(8-x)f_d, f_{ad} = 0.5(x-6)f_d$	$f_{bd} = f_d$
8–10 mm	$f_{ad} = f_d$	$f_{bd} = 0.5(10-x)f_d, f_{cd} = 0.5(x-8)f_d$
10–12 mm	$f_{ad} = 0.5(12-x)f_d, f_{bd} = 0.5(x-10)f_d$	$f_{cd} = f_d$

The force sharing strategy can be performed by an FDF

$$\mathrm{FDF}(x, f_\mathrm{d}) = f_\mathrm{d}[w_a(x) \quad w_b(x) \quad w_c(x)] \tag{11}$$

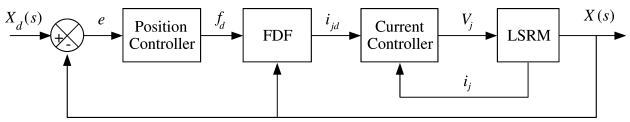

Fig. 4 The block diagram for the structure of the whole control system

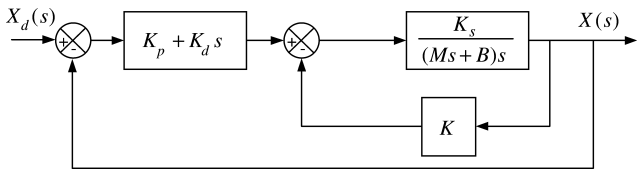

Fig. 5 The block diagram for the modified PD controller

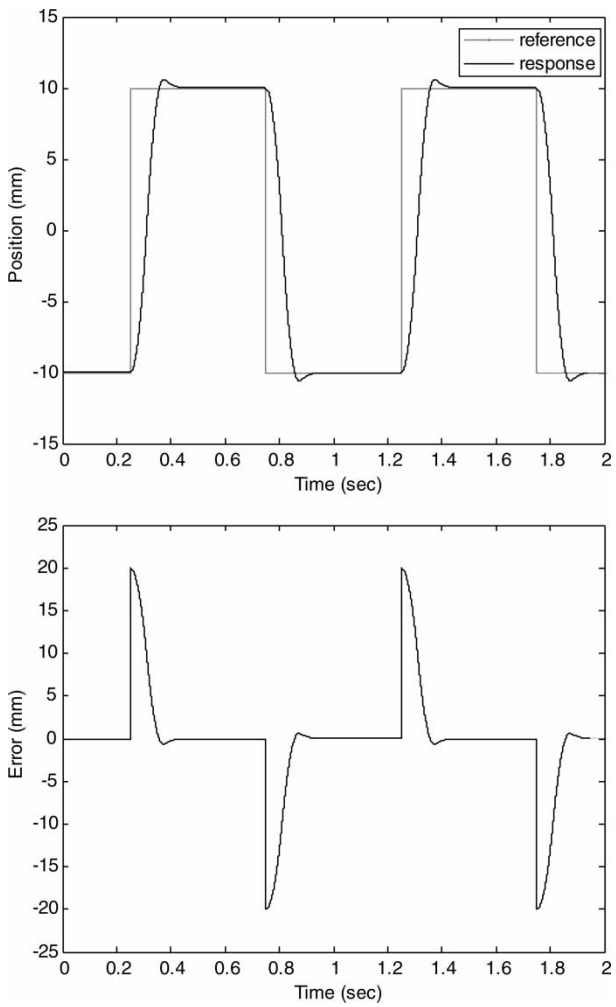

Fig. 6 Simulation profile of square wave tracking under a PD control ($K_\mathrm{p} = 8$, $K_\mathrm{d} = 0.24$)

where f_d denotes the desired total force and w_j denotes the weighting of force for phase j. An FDF should in addition satisfy the principles as follows

$$\begin{cases} f_\mathrm{d} \geqslant 0, w_j(x) > 0 \; \forall j \in \Theta^+ \text{ and } w_j(x) = 0 \; \forall j \in \Theta^- \\ f_\mathrm{d} < 0, w_j(x) > 0 \; \forall j \in \Theta^- \text{ and } w_j(x) = 0 \; \forall j \in \Theta^+ \end{cases} \tag{12}$$

$$\sum_{j=a}^{c} w_j(x) = 1 \tag{13}$$

The selection of *weighting* depends on the various force sharing strategies influencing their design considerations. A phase inductance ratio-based FDF is proposed for the phase current transition during its commutation in reference [**8**]. A simpler FDF scheme is proposed using a linear switching in reference [**11**]. However, all force sharing strategies should satisfy the condition that the sum of each weighting should be 1, which means that the sum of each phase force agrees with the desired total force.

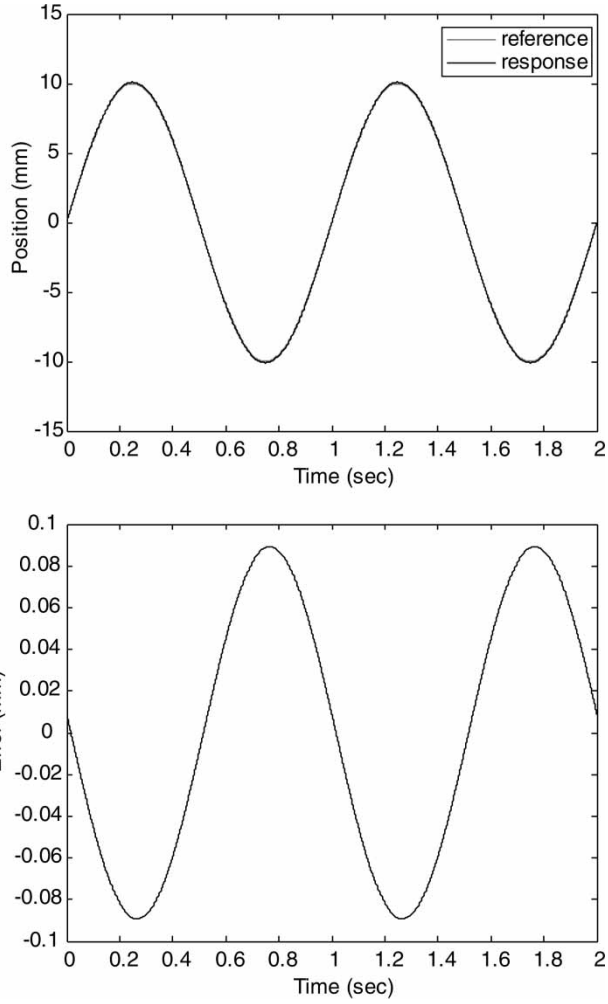

Fig. 7 Simulation profile of square wave tracking under a PD control ($K_\mathrm{p} = 8$, $K_\mathrm{d} = 0.24$)

According to the force produced function in equation (6), the desired phase currents can be calculated by the output of the applied FDF and function of the inductance ratio. The precise model for flux linkage is hard to obtain due to its inherent complexity. To calculate the desired phase currents, the non-linear magnetic characteristics are usually approximated by a ratio function of phase inductance to displacement. A few methods have been proposed for approximating this ratio function, which can be classified into two groups: through a lookup table [**3**, **11**] and through an approximation function [**4**, **14**]. The lookup table needs only memory to store the characteristic data from the actual measurements; however, it lacks flexibility. The approximation function needs more mathematical processing; but is more flexible for practical use.

As the linkage between the electrical sub-system and mechanical sub-system, an FDF and an approximation function of an inductance ratio are together referred to as motor winding excitation scheme. The diagram of a motor winding excitation scheme is represented in Fig. 2. The FDF is used to compute the desired phase force according to the position and the desired total force. The approximation function of the inductance ratio is used to compute the desired phase current by using the desired phase force and position.

The applied FDF in this article is chosen as in Table 2 as the Table 3 in reference [**11**] and the approximation function of the inductance ratio is described in a sinusoidal function of position in reference [**14**]. The corresponding experimental results of force produced for a single phase and the force sharing strategy performed on the proposed LSRM are given by Fig. 3. The figure of single phase shows the highly non-linear force characteristics of the LSRM. From the

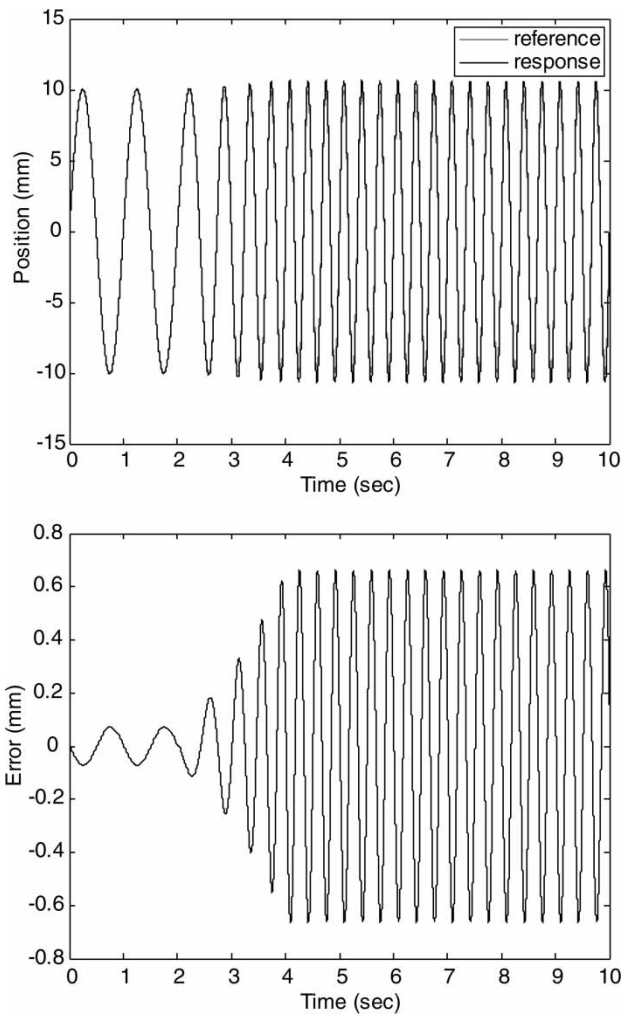

Fig. 8 Simulation profile of sinusoidal wave tracking under a PD control with frequency of input signal increasing ($K_p = 8$, $K_d = 0.24$)

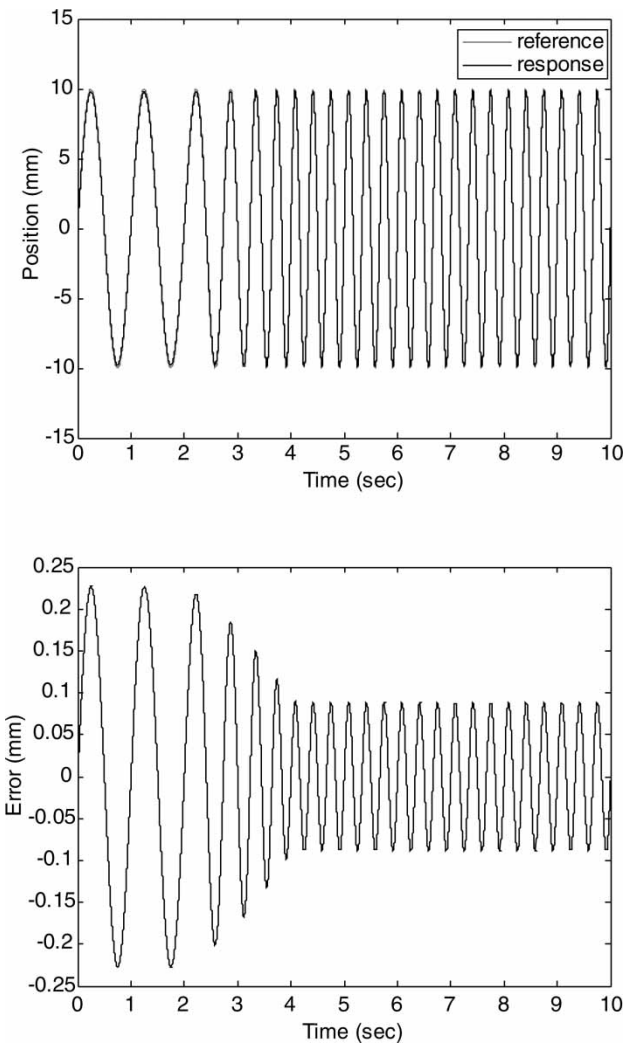

Fig. 9 Simulation profile of sinusoidal wave tracking under a modified PD control with frequency of input signal increasing ($K_p = 40$, $K_d = 0.24$, $K = 1$)

experimental figure of force sharing strategy, it can be clearly seen that the non-linearities are reduced greatly even though there are still some ripples in the force outputs.

2.3 Controller design

The driving system adopts a cascaded control structure, two controllers are designed for the electromagnetic subsystem and the mechanical subsystem corresponded to current control and position control, respectively. The applied FDF in the middle of the two control subsystems. The block diagram of the whole driving system is shown as Fig. 4. In the cascaded control system, the inner loop is for current control with fast variables and the outer loop is for the position control with slow variables.

For each phase coil, the relationship from terminal voltage to phase current can be represented as equation (14) by the rearrangement of equation (3). R_j is treated as a generalized resistor. Hence, the dynamic behaviour of the electromagnetic subsystem can be approximated as a first-order differential equation. As the inner loop, it can be easily regulated by a proportional controller to guarantee both stability and quick response

$$L_j \frac{\mathrm{d}i_j}{\mathrm{d}t} = V_j - R_j i_j, \qquad R_j = r_j + \frac{\mathrm{d}L_j}{\mathrm{d}x}\frac{\mathrm{d}x}{\mathrm{d}t} \tag{14}$$

$$G(s) = \frac{K_\mathrm{s}}{(Ms + B)s} \tag{15}$$

Note that if the inner loop is to impose perfect current tracking, the mechanical subsystem can be equivalently represented by a transfer function as a second-order system equation (15), where K_s denotes the system gain. In this article, the system gain is 1000. Suppose there is no external load, a simple PD controller as in equation (16) is sufficient for the position tracking and its closed-loop transfer function is given

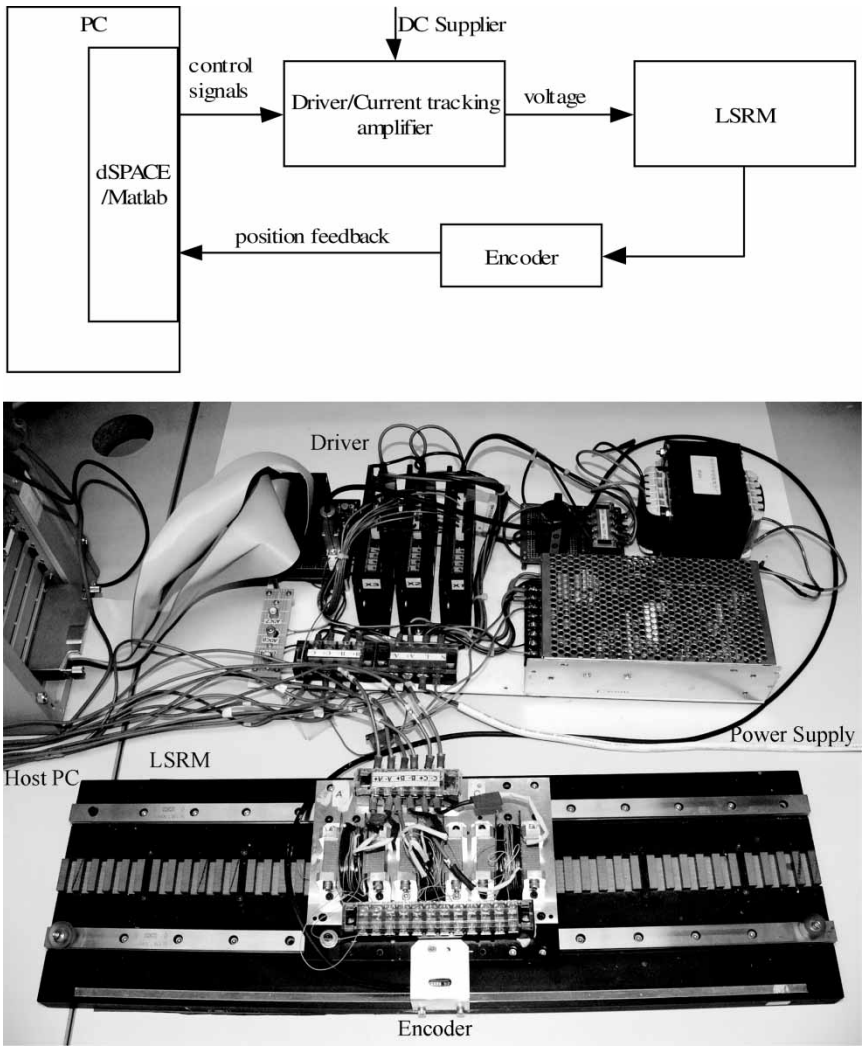

Fig. 10 Experimental set-up of the driving system

by equation (17)

$$C(s) = K_p + K_d s \tag{16}$$

$$\frac{X(s)}{X_d(s)} = \frac{K_s(K_p + K_d s)}{Ms^2 + (K_s K_d + B)s + K_s K_p} \tag{17}$$

where K_p and K_d are the proportional gain and differential gain of the controller, respectively. Under the PD control, the system stability and high performance can be achieved by adjusting its controller parameters. However, for certain special applications such as continuous sinusoid tracking, the tracking error is sensitive to the frequency of input

$$\frac{E(s)}{X_d(s)} = \frac{Ms^2 + Bs}{Ms^2 + (K_s K_d + B)s + K_s K_p} \tag{18}$$

$$\frac{E(s)}{X_d(s)} \approx \frac{Ms^2 + Bs}{K_s K_p} \tag{19}$$

The error-input transfer function of this system is described in equation (14). To meet the dynamic response requirements, the proportional gain K_p is often set at a high value while the differential gain K_d is small. In the low-frequency band, equation (18) can be approximated as equation (19) because of $K_s K_p \gg Ms^2 + (K_s K_d + B)s$. It can be seen that the error-input transfer function acts a high-pass filter.

The error-input transfer function can also be designed as a low-pass filter when the position controller is modified as in Fig. 5, where K is the gain of inner loop. In this case, the system is described as equation (20) and the error-input transfer function is given by equation (21). If K are chosen properly that $K_s K \gg Ms^2 + Bs$, the error-input transfer function can be approximated as equation (22) in the low-frequency band. It acts as a low pass filter and the bandwidth increases with

$$\frac{X(s)}{X_d(s)} = \frac{K_s(K_p + K_d s)}{Ms^2 + (K_s K_d + B)s + K_s(K + K_p)} \tag{20}$$

$$\frac{E(s)}{X_d(s)} = \frac{Ms^2 + Bs + K_s K}{Ms^2 + (K_s K_d + B)s + K_s(K + K_p)} \tag{21}$$

$$\frac{E(s)}{X_d(s)} \approx \frac{K_s K}{Ms^2 + (K_s K_d + B)s + K_s(K + K_p)} \tag{22}$$

3 SIMULATION RESULTS

The simulations are achieved with the MATLAB software package and illustrated in this section. The simulation results first demonstrate the track performances of a PD controller for a square wave and a sinusoidal wave. Next the response profiles for sinusoidal wave of the PD controller are compared with those of a modified PD controller at different frequencies.

The position responses of a square wave and a sinusoidal wave for PD controller are shown in Figs 6 and 7, respectively. In these figures, the maximum distance is 20 mm and the frequency is 1 Hz. It can be seen that the LSRM driving system has good dynamic performance with zero steady-state error.

The position response of the sinusoidal wave is shown in Fig. 8 for the PD controller with its frequency increase from 1.0 to 3.0 Hz. Note that in this case, the peak-to-peak error increases rapidly from about 0.2 to 0.6 mm as frequency increases. The corresponding experimental result for the modified PD controller is shown in Fig. 9. Compared with the former, it is clear that the peak-to-peak error decreases slowly as frequency increases. The simulation results demonstrate that the modified algorithm is insensitive to the variation of the frequency.

4 EXPERIMENTAL IMPLEMENTATIONS

The diagrammatic sketch and the actual experimental set-up of the driving system are shown in Fig. 10.

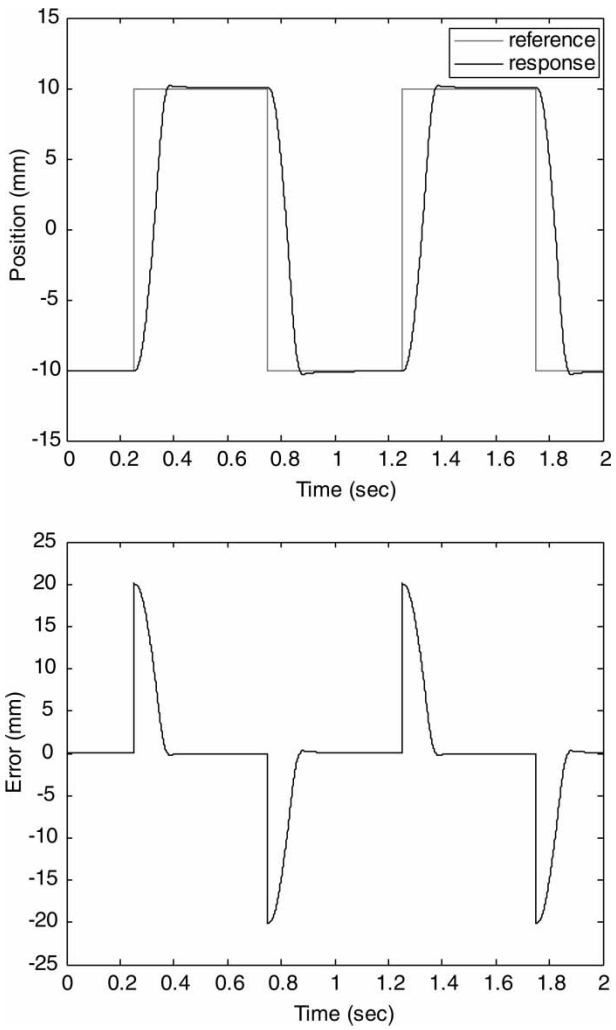

Fig. 11 Experimental response of square wave tracking under a PD control ($K_p = 8$, $K_d = 0.24$)

The host PC is a Pentium 4 computer that is used to download the target code into a dSPACE DS1104 DSP motion controller card, and supports an interface to adjust the system parameters in real-time. The control algorithm is developed using MATLAB/SIMULINK. All control functions are implemented and state variables are sampled by the DS1104 card, which is plugged into a PCI bus of the host PC. Note that the experimental set-up is intended for the purpose of development. In applications, the proposed control scheme can be fully implemented by a low-cost embedded system. The driver consists of three asymmetric bridge IGBT inverters with a DC voltage supplier corresponding to the three winding, respectively. A linear optical encoder with 0.5 μm resolution is mounted on the mover of the LSRM system and provides position feedback information.

In the whole driving system, the current tracking requires high-speed response but has relatively simple control, while the position control and the FDF are relatively slow but complicated. Therefore, the current control is performed by an analogue amplifier hardware in order to meet its speed requirements. The micro-computer system is used to realize to the position controller and FDF. The merits of this arrangement are (a) flexibility of implementation and application, and (b) optimized performance of the micro-processor system. In this experimental system, current control is implemented by a commercial driver with 20 kHz switching frequency. The selection of sampling frequency for the position control is dependent upon the required system performances and hardware limitations. Generally speaking, a sampling frequency ranging from 1 to 2 kHz can achieve a good position tracking. In this system, the sampling frequency is chosen as 1 kHz.

The position responses of square wave and sinusoidal wave for PD controller are shown in Figs 11

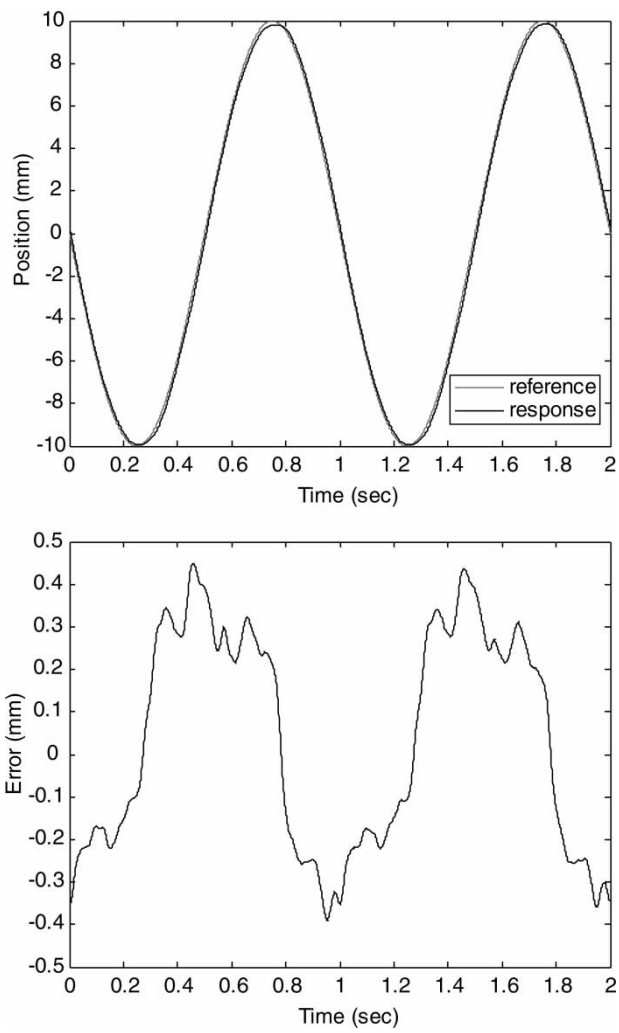

Fig. 12 Experimental response of sinusoidal wave tracking under a PD control ($K_p = 8$, $K_d = 0.24$)

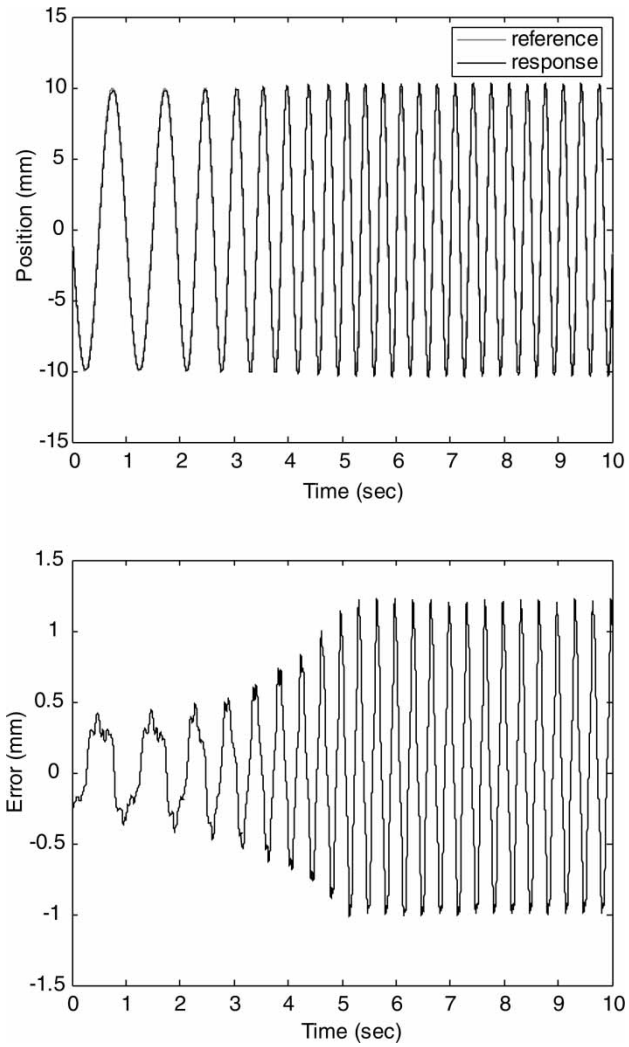

Fig. 13 Experimental response of sinusoidal wave tracking under a PD control with frequency of input signal increasing ($K_p = 8$, $K_d = 0.24$)

and 12, respectively. In these figures, the maximum distance is 20 mm and the frequency is 1 Hz. It can be seen that the LSRM driving system has good dynamic performance with zero steady-state error.

The position response of the sinusoidal wave is shown in Fig. 13 for the PD controller with its frequency increase from 1.0 to 3.0 Hz. Note that in this case, the peak-to-peak error increases rapidly from about 0.4 to 1.2 mm as frequency increases. The corresponding experimental result for the modified PD controller is shown in Fig. 14. Compared with the former, it is clear that the peak-to-peak error decreases slowly as frequency increases. As with the simulations, the experimental results also demonstrate that the modified algorithm is robust to the variation of the frequency.

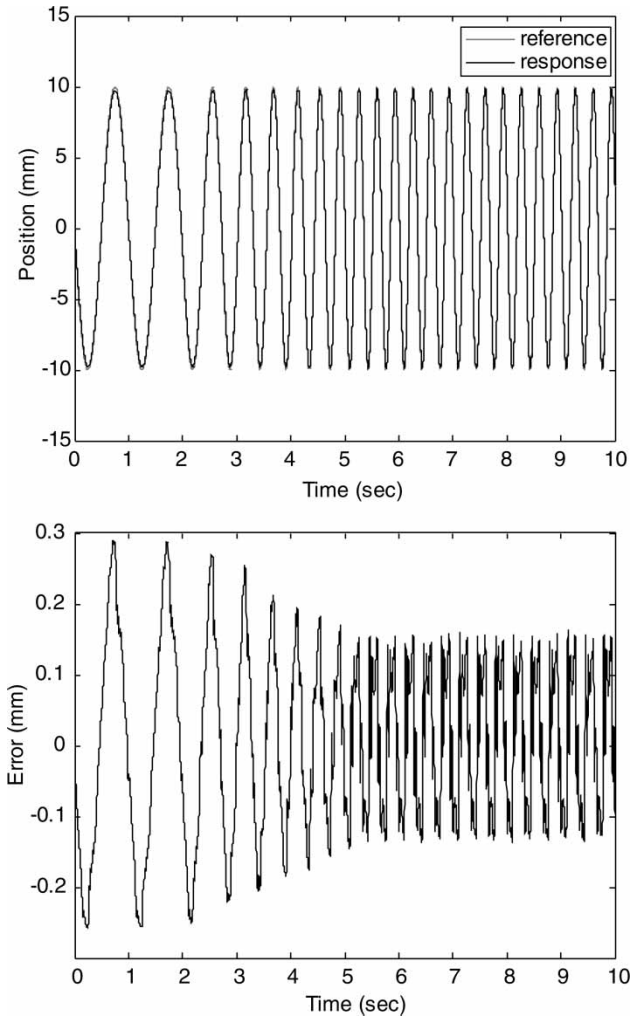

Fig. 14 Experimental response of sinusoidal wave tracking under a modified PD control with frequency of input signal increasing ($K_p = 40$, $K_d = 0.24$, $K = 1$)

5 CONCLUSION

In this article, a simple yet effective design of feedback control is represented for trajectory control of the LSRM driving system. Based on the two-time-scale analysis, the driving system is decomposed into two reduced-order subsystems with two different time scales. According to that the position controller and the current controller are designed for the two subsystems, respectively. The entire control system adopts a cascaded structure and the inner loop and outer loop are connected by the FDF. This control scheme simplifies the controller design and makes the tracking system implementation tractable. Furthermore, a modified PD controller is proposed to enhance the system performance for the tracking of sinusoid waves. Simulations and experimental results verify that the model and control algorithm of the LSRM is efficient and effective.

ACKNOWLEDGEMENTS

The work described in this paper was fully supported by a grant from the Research Grants Council of the Hong Kong Special Administrative Region, China (PolyU 5224/04E). The authors would also like to thank the general support of South China University of Technology through National Natural Science Foundation of China (60674099).

REFERENCES

1 **Lawrenson, P. J., Stephenson, J. M., Blenkinsop, P. T., Corda, J.,** and **Fulton, N. N.** Variable-speed switched reluctance motors. *IEE Proc. Electr. Power Appl.*, 1980, **127**(4), 253–265.

2 **Barrass, P. G.** and **Mecrow, B. C.** Flux and torque control of switched reluctance machines. *IEE Proc. Electr. Power Appl.*, 1998, **145**(6), 519–527.

3 **Taylor, D. G.** An experimental study on composite control of switched reluctance motors. *IEEE Control Syst. Mag.*, 1991, **11**(2), 31–36.

4 **Ilic'-Spong, M., Marino, R., Peresada, S. M.,** and **Taylor, D. G.** Feedback linearizing control of switched reluctance motors. *IEEE Trans. Autom. Control*, 1987, **AC-32**, 371–379.

5 **Panda, S. K.** and **Dash, P. K.** Application of non-linear control to switched reluctance motors: a feedback linearization approach. *IEE Proc. Electr. Power Appl.*, 1996, **143**(5), 371–379.

6 **Bortoff, S. A., Kohan, R. R.,** and **Milman, R.** Adaptive control of variable reluctance motors: a spline function approach. *IEEE Trans. Ind. Electron.*, 1998, **45**(3), 433–444.

7 **Milman, R.** and **Bortoff, S. A.** Observer-based adaptive control of a variable reluctance motor: experimental results. *IEEE Trans. Control Syst. Technol.*, 1999, **7**(5), 613–621.

8 **Bae, H. K., Lee, B. S., Vijayraghavan, P.,** and **Krishnan, R.** A linear switched reluctance motor: converter and control. *IEEE Trans. Ind. Appl.*, 2000, **36**(5), 1351–1359.

9 **Dorningos, J. L., Andrade, D. A., Freitas, M. A. A.,** and **De Paula, H.** A new drive strategy for a linear switched reluctance motor. In the Electric Machines and Drives Conference, Madison, Wisconsin, USA, 2003 (IEMDC'03), June 2003, vol. 3, pp. 1714–1719.

10 **Pan, J. F., Kwok, S. C., Cheung, N. C.,** and **Yang, J. M.** Auto disturbance rejection speed control of linear switched reluctance motor. In the Industry Applications Conference, (IAS'05), Hong Kong, China, October 2005, vol. 4, pp. 2491–2497.

11 **Gan, W. C., Cheung, N. C.,** and **Qiu, L.** Position control of linear switched reluctance motors for high-precision applications. *IEEE Trans. Ind. Appl.*, 2003, **39**(5), 1350–1362.

12 **Gan, W. C., Cheung, N. C.,** and **Qiu, L.** Short distance position control for linear switched reluctance motors: a plug-in robust compensator approach. In the IEEE Industry Applications Conference, Chicago, Illinois, USA, September/October 2001, vol. 4, pp. 2329–2336.

13 **Majmudar, H.** *Electromechanical energy converters*, 1965 (Allyn and Bacon, Inc., Boston).

14 **Khorrami, F., Krishnamurthy, P.,** and **Melkote, H.** *Modeling and adaptive non-linear control of electric motors*, 2003 (Springer, Germany).